WILEY-VCH

Chipset nanosensor based on N-doped carbon nanobuds for selective screening of epinephrine in human samples

Mohammed Y. Emran[1], Sherif A. El-Safty[1,*], Ahmed Elmarakbi[2], Abduallah Reda[1], Ayman EL Sabagh[3], Mohamed A. Shenashen[1]

[1] National Institute for Materials Science (NIMS), Research Center for Functional Materials, 1-2-1 Sengen, Tsukuba-shi, Ibaraki-ken 305-0047, Japan

[2] Faculty of Engineering and Environment, Northumbria University, Newcastle upon Tyne, NE1 8ST, UK

[3] Department of Field Crops, Faculty of Agriculture, Siirt University, Siirt, Turkey

*Correspondence: sherif.elsafty@nims.go.jp

Homepage: https://samurai.nims.go.jp/profiles/sherif_elsafty

Keywords: Portable nanosensor; Nitrogen doped carbon-based materials; Functionalized electrode; Electrochemical sensors/biosensors; Advanced nanocarbon materials; Sensitive and selective epinephrine assay

Abstract

Chipset nanosensor design and fabrication are important for healthcare research and development. Herein, A functionalized chipset nanosensor is designed to monitor neurotransmitters (i.e., epinephrine [EP]) in human fluids. An interdigitated electrode array (IDA) is functionalized by N-doped carbon nanobuds (N-CNB) and N-doped carbon nanostructures (N-CNS). The surface morphology of N-CNB shows the formation of nanotubular-like branches on sheets and micrometric-sized tubes. The N-CNS design consists of the formation of aggregated sheets and particles in nanometric size. The irregular shape formation provides surface heterogeneity and numerous free spaces between the stacked nanostructures. N-atoms ascertains highly active N-CNS with multi-functional active centers, electron-rich charged surface, and short distance pathway. The N-CNB/IDA exhibits the best performance for EP signaling with high sensitivity and selectivity. The N-CNB/IDA sensing performance for EP detection indicates the successful design of a highly selective and sensitive assay with low detection limit of 0.011 µM and a broad linear range of 0.5 – 3 µM. The N-CNB/IDA exhibits a high degree of accuracy and reproducibility with RSD of 2.7% and 3.9%, respectively. Therefore, the chipset nanosensor of N-CNB/IDA can be used for on-site monitoring of EP in human serum samples and further used in daily monitoring of neuronal disorders.

1. Introduction

Portable and disposable sensors/biosensors are an important topic in advanced healthcare and environmental analytical assays. The development of portable sensors/biosensors needs the combination and accomplishment of various fields, such as material science, electrochemical, optical, biotechnology, and engineering [1]. Material science plays a key role in producing economical and highly stable devices for target monitoring. The material components of sensor devices advance the sensor performance and usability, enhance signaling stability, produce low-cost devices, and integrate environmental impacts [1-2]. Portable electrochemical devices are regarded as potential analytical techniques for sensing and biosensing of various targets such as bacteria, viruses, pesticides, and glucose [3]. Electrodes are the major component of electrochemical devices; thus, their easy fabrication by using various techniques with highly active materials can be performed on portable chips [2b, 4]. The operation process using electrochemical instruments involves a low power consumption, simple operation, detection of various targets, and portable/on-site use [5]. Therefore, electrochemical devices have been widely designed/approached for commercial use.

Portable devices based on electrochemistry depend on the design and fabrication of a three-electrode system in one chip, such as screen-printed electrodes (SPE) and an interdigitated electrode array (IDA). The chipset design contains three electrodes, namely, the working, reference, and auxiliary electrodes, in one chip, whereas a designed chip contacts the potentiostat using one USB-like cable [6]. The IDA acts as a chipset sensor-based device, and it has been used for biosensing applications. The surface functionalization of IDA occurs by immobilization of bioreactors (i.e., antibodies, aptamers, and whole cells) on its surface (i.e., metallic surface of Au-based working IDA) [7]. Numerous approaches have used IDA-based electrodes for the design of lab-on-chip (LOC) devices. In this context, LOC was designed to detect ovarian cancer cells (SKOV3) by a continuous microfluidic chip through the IDA working area. Ovarian cancer was detected using LOC-based devices through impedimetric

measurements after continuous blood separation and specific capture of cancer cells from the extracted plasma [8]. An LOC-based device was used for electrochemical sensing of glucose, lactate, and uric acid (UA) in human blood samples [9]. A portable cortisol immunosensor was designed based on the immobilization of cortisol antibodies on the surface of IDA electrodes. Impedimetric signaling was used for the detection process with high sensitivity and accuracy in saliva samples [7a]. The production of portable sensors/biosensors with a combination of technologies (i.e., engineering and electrochemical sensors) for reading out various targets in resources and receptors is highly required. Therefore, the integration and functionalization of IDAs for reading out targets, such as neurotransmitters, remains a challenge for voltametric, impedimetric, and amperometric applications.

The advance development of nanomaterials that used for electrode modification and functionalization have been attained a great interest in academic and industrial fields. The nanomaterials composition and morphology play a vital role in the sensing and biosensing sensitivity and selectivity such as signaling of neurotransmitters, ascorbic acid (AA), uric acid (UA), glucose, pesticides, viruses, and H_2O_2 [3, 10]. Carbon-based material synthesis and functionalization with a simple and low-cost approach with advantages of fast fabrication, eco-friendliness, high stability, reproducible nanostructure, and multi-functional active surface have aroused great interest [11]. Heterogeneous doping of carbon materials by B, N, P, and S atoms enhances functionality and electrochemical properties and produces a highly active catalytic surface for various biosensors and energy applications [11a, 12]. Functionalized carbon materials (i.e., heterogeneously doped graphene, carbon nanotubes, and carbon spheres) have been widely used as active surface mediators for signaling epinephrine (EP). Nitrogen atoms/sources are widely used for doping of carbon materials (i.e., graphene, carbon nanotubes, and carbon spheres). The N atoms act as n-type dopant; they enhance the electrochemical activity of carbon materials and produce a heterogeneous multi-functional electrode surface [12h, 13]. As a result, doping of carbon materials with N atoms has sparked considerable interest as a means to

develop active materials with good electrochemical, mechanical, and optical properties. Therefore, N-doped carbon materials with high stability and reusability can be used for responsive and selective signaling of different targets (e.g., EP).

Neurotransmitters (i.e., dopamine, epinephrine (EP), and norepinephrine) monitoring is one of the potential fields of neuronal disorder studies (i.e., neuronal behavior, medical treatment, and clinical investigation) [5c]. EP molecules are usually secreted in human fluids through the adrenal gland during fight/flight situations [14]. The key role of EP molecules in the human body is associated with the transmission of neuronal signaling, enhancement of O_2 and glucose supply in emergency states, and further utilization in intensive care units for the treatment of heart diseases, anaphylactic shock, and asthma [15]. The EP level in human fluids, brain, and neuronal tissue can be used as a biomarker of neuronal disorders, such as schizophrenia syndrome, Alzheimer's, and Parkinson's disease [16]. The analytical detection of EP has been approached using various methods, such as chromatography, chemiluminescence, fluorimetry, spectrophotometry, electrochemiluminescence, flow injection, and electrochemical techniques [14c, 14d, 17]. The advantages of electrochemical techniques include a high signaling amplification, easy use, short response time, manageable portable-based biosensors, and on-site detection without further procedures [10a, 14c, 14d]. A portable electrochemical sensor design with sensitive and selective signaling for targets, high stability and reproducibility, and can be easily used for in-vitro and in-vivo applications is highly required for quantitative signaling of biomolecules in their resources and receptors (i.e., EP in human blood samples) [11b, 14a, 14b]. The use of highly active materials with novel structural and electrochemical properties for the function and/or fabrication of an IDA working surface presents a challenge. Therefore, the production and development of LOC-based devices for selective monitoring of EP sensors are highly required for clinical investigation and early diagnosis of neuronal disorders.

Herein, we designed a portable sensor based on the fabrication and modification of chipset IDA for advanced portable healthcare devices. The chipset nanosensor composed of N-doped carbon

nanobud (N-CNB)- and N-doped carbon nanostructure (N-CNS)-functionalized IDA electrodes were designed to detect EP in human fluid samples. N-CNB and N-CNS were synthesized using a simple approach and controlled self-assembly. The formation of N-CNB was controlled at the sheet level and micrometric tube-like base surface. The nanobuds were grown vertically to form a tubular branched-like structure that formed a heterogeneous surface with multiple V-shaped free spaces, grooves, and heterogeneous angularities. These features induced electrolyte diffusion through the base surface and around the nanobuds and created a wide contact surface interface area. In addition, the presence of N atoms in the graphitic carbon chain improved electrochemical activities, such as fast charge transport, high catalytic activity, and charge surface, due to various pyrrolic groups, including pyridinic and graphitic N. The designed chipset nanosensor of N-CNS/IDA exhibited a good sensitive and selective response to EP with high signaling stability and reproducibility. Thus, the N-CNB/IDA was successfully designed to screen EP in human samples, and it can be used as a portable sensor for advanced healthcare devices.

2. Results and discussion

A portable sensitive and selective assay of neurotransmitters was designed based on the functionalization of the chipset nanosensor of IDA. The IDA electrode surface configures the highly stable working chip to transduce electrochemical signals with high sensitivity. The IDA was modified by N-CNB and N-CNS to ascertain a highly active and specific EP sensor. The surface composition and morphology provided a highly active mediator that can be employed to detect a specific target with high signaling transduction, low power consumption, on-site detection, and low sample volume. The key points of N-CNB surface morphology (i.e., the foundation of various heterogeneous angularities, rough surface texture, multiple free spaces, and V-shapes) enabled molecular diffusion throughout the inner/outer surface, increased the mass-to-volume ration, and induced target loading at the electrode surface. In addition, the

surface morphology of N-CNB formed a 3D chelate-like structure with rough and ridged ends that enlarged the electrode mechanical stability and enhanced the stability and reusability of the chipset nanosensor. Moreover, the chemical composition of N-CNB (N-doped Sp^2 carbon chain) led to the creation of a new functional surface with fast charge transport, high electron diffusion pathway, foundation plane edge defects, and the existence of a partially negatively charged surface with a pool of electrons [18].

We controlled the synthesis of N-doped carbon nanomaterials using a simple, one-pot approach. The N-CNB and N-CNS structures were produced by hydrothermal treatment (HT) of glucose and UA in the presence of a capping agent (Scheme 1). The HT of glucose molecules usually produces micrometer-sized carbon spheres. At a high temperature of 180 °C, glucose is condensed, polymerized, and aromatized in a series of steps [19]. UA acted as a N dopant source and may serve as the directing agent for producing N-CNB, whereas aminobenzoic acid served as the N atom source and directing agent of N-CNS. For NCB, UA played a key role in the nanobud structure formation. Organonitrogen compounds, such as UA, phenylenediamine, guanine, adenine, and thymine (high nitrogen contents), are regarded as sources of N atoms through graphitization and formation of graphitic carbon nitrides and N-doped graphene and multi-walled carbon nanotubes [20]. The decomposition of UA and the combination of heterocyclic -NH group of UA during the polymerization and aromatization of glucose formed N-doped carbon materials [20a, 21]. The same interaction of glucose and aminobenzoic acid occurred under the HT condition, and the N-CNS was formed. UA and aminobenzoic acid controlled the formation of carbon materials with various morphologies of carbon nanobuds and nanostructures. Pluronic F127 acts as the directing agent of morphology and porous structure. The presence of F127 (tri-block F127 (EOx-POy-EOx)) in the carbonization of glucose, UA, and aminobenzoic acid led to the controlled formation of N-CNB and N-CNS [22]. Therefore, F127 controlled the aggregation and porous formation of N-CNB and N-CNS [12c].

The synthesized materials were annealed at high temperatures (800 °C) under N_2 flow to form N-CNB and N-CNS.

Scheme 1

The surface morphology and topography of N-CNB and N-CNS were examined using field emission-scanning electron microscopy (FE-SEM). Figure 1A shows the FE-SEM images of N-CNB on various sections and under different magnifications. The surface morphology of N-CNB exhibited surface heterogeneity and buildup of carbon nanobuds (Figure 1Aa). The buds formed and grew as tubes on carbon sheets and branched-like structure (Figures 1Aa and 1Ac). The buds attached to the surface, interlinked with the carbon sheet surface, and formed a tube-like branch. The formed bud had a nanometric size of 70–150 nm and various lengths (Figure 1Ab). In addition, the various sizes and lengths of the buds transformed the surface to a heterogeneous one with multiple grooves, zigzag orientation, wave-like view, rough surface, and up/down movements. Figure 1Ac shows the cross-section of N-CNB and bud formation on the sheet and micrometer-size tube-like structures. The highly magnified FE-SEM image showed a bud growth similar to that of branches of a tree trunk. Figure 1Ad shows the N-CNB surface heterogeneity and roughness with various bud sizes and lengths. The N-CNB structure showed various surface defects, including V-shaped free spaces, heterogenous angularities, and 3D bud growth. The elemental analysis was carried out using energy-dispersive X-ray spectroscopy (EDX)-SEM mapping (Figure 1B). The elemental mapping of N-CNB indicated that the N-CNB was composed of C, N, and O with % wt of 82.33%, 7.1 %, and 10.57 %, respectively (Figures 1Ba–1Bc). Therefore, the synthesized carbon materials of N-CNB contained O and N in the form of a carbon chain (graphitic carbon). Figure 2A shows the FE-SEM images of N-CNS. Figure 1Aa shows the overall view of the N-CNS structure. Stacked irregularly shaped nanometer-sized aggregated sheets and particles were observed. Figure 2Ab shows the cross-section of the N-CNS structure. The aggregated sheets and particle size were in the range of 70–200 nm (inset in Figure 2Ab). Moreover, the N-CNB contained numerous

free spaces between the nanostructures, resembling grooves. Figure 2B(a–c) show the EDX-SEM mapping of N-CNS. The N-CNS was composed of C, N, and O with % wt of 83.5 %, 6.2 %, and 10.3 %, respectively. Thus, the N-CNB and N-CNS materials contained N and O atoms that played key roles in the functionalization and electrochemical properties of these materials.

Figure 1

The surface nature, composition, and crystalline formation of N-CNB and N-CNS were investigated using various techniques, including X-ray photoelectron spectroscopy (XPS), Raman shift, N_2–adsorption isotherm, and X-ray diffraction (XRD). Figure 2C shows the N_2 adsorption isotherm of N-CNB (violet line) and N-CNS (wine line). The N-CNB followed a type I isotherm, which presented a dominant microporous network, whereas the N-CNS exhibited the type IV isotherm and illustrated the formation of a dominant mesoporous network [23]. The Brunauer–Emmett–Teller surface areas (S_{BET}) were 45.3 and 6.54 m^2g^{-1} for N-CNB and N-CNS, respectively. The nonlocal density functional theory was applied to confirm the pore size distribution (Figure S1A). The pore size and volume of N-CNB (dp = 2.08 nm and Vp = 0.042 cm^3g^{-1}) and N-CNS (dp = 12, 28 nm and Vp = 0.0057 cm^3g^{-1}) presented a porous network formation containing meso- and micropores. Figure S1B shows the Raman shift spectra of N-CNB (wine line) and N-CNS (violet line). Two broad peaks of D and G bands were centered at 1354.4 and 1612.6 cm^{-1}, respectively. The D and G bands indicated the carbon sp^3 (distortion of graphitic carbon) and sp^2 (linear graphitic sp^2 hybridization) hybridizations, respectively [24]. Furthermore, the I_D/I_G values of N-CNB (0.94) and N-CNS (0.97) indicated the degree and effect of dopant atoms and the graphic characteristics of carbons, confirmed the heteroatom (N and O) doping of the graphical carbon chain, and proved the formation of several plane edge defects. Figure S1C shows the wide-angle XRD pattern of N-CNB (wine line) and

N-CNS (violet line). Two XRD peaks centered at 2θ of 29.1° and 41.2° were located based on the 002 and 100 crystal planes, respectively, indicating the formation of carbon materials [25]. Figure S1D shows the XPS spectrum of N-CNB. Three XPS peaks were observed at 533.12, 392.33, and 284.01 eV for O 1s, N 1s, and C 1s, respectively. The XPS survey of C 1s indicated the various carbon bond types, namely, C–O/C–N, C–C (sp^3), O–C=O, and C–C (sp^2) at 289.51, 285.75, 288.2, and 285.04, eV, respectively (Figure S1E). These kinds of bonds ascertained the formation heteroatom-doped carbon-based material with the successive aromatization and carbonization of poly-glucose and active functionalized surface formation due to the presence of O and N in N-CNB. Figure 2D shows the XPS survey of N 1s, where four peaks centered at 299.13, 398.21, 400.4, and 402.9 eV corresponded to pyrrolic, pyridinic, quaternary, and graphitic and oxidized N, respectively [14c, 26]. The XPS survey of O 1s showed three XPS peaks at 530.9, 531.98, and 532.9 eV and signified the presence of quinone-type (C=O), phenol-type (C–OH), and groups (C–O–C and C–O–OH), respectively (Figure S1F). Therefore, the N-CNB composition provided an active functional surface design with high electron mobility/contents and surface wettability, enhancing the material selectivity, strong target binding, and fast charge transport.

Figure 2

2.1 Catalytic activity and sensing property of the chipset nanosensor based on N-CNB/ IDA and N-CNS/IDA

The chipset nanosensor electrocatalytic of N-CNB/ IDA and N-CNS/IDA activity was investigated using CV. Figure 3A shows the CV values of various chipset electrodes of IDA (a), N-CNS/IDA (b), and N-CNB/IDA (c) in $[Fe(CN)_6]^{3-/4-}$ solution. Quasi-reversible redox peaks with various current peak values and potential positions were observed. The redox peak current values and the corresponding potential position of $Fe^{2+/3+}$ refer to the catalytic surface and charge transport on the designed chipset electrodes, respectively. The anodic current values were 9.45, 25.04, and 49.94 µA for IDA, N-CNS/IDA, and N-CNB/IDA, respectively. The ΔE

values (the difference between the anodic and cathodic peak position values) were 210 (IDA), 178 (N-CNS/IDA), and 90 (N-CNB/IDA) mV. Thus, the designed chipset electrode of N-CNB/IDA showed the highest catalytic activity and fastest electron transfer compared with the other electrodes [27]. This finding may be related to the surface morphology, surface nature, and chemical composition of N-CNB. The Rundles–Sevick formula can be used to calculate the active electrode surface area [28]:

$I_p(A) = 2.69\times10^5\, n^{3/2} A_0 D_0^{1/2} C_0 \nu^{1/2}$

where A represents the surface area of the electrode (cm^2), D_o denotes the diffusion coefficient ($cm^2\ s^{-1}$), I_p refers to the anodic peak current(A), n indicates the electron transfer number, C_o stands for the concentration of $[K_3Fe(CN)_6]$ (mol cm^{-3}), and ν is the scan rate (Vs^{-1}). The calculated surface areas of IDA, N-CNS/IDA, and N-CNB/IDA were 3.5×10^{-4}, 9.5×10^{-4}, and 19.1×10^{-4} cm^2, respectively.

Figure 3B shows the electrochemical impedance spectroscopy (EIS) (Nyquist mode) in $[Fe(CN)_6]^{3-/4-}$ solution for IDA (a), N-CNS/IDA (b), and N-CNB/IDA (c). The semicircle Nyquist mode at high frequency and the line at low frequency indicate the surface charge resistance (Res) and electron diffusion velocity of the chipset electrodes [11b, 11c]. The N-CNB/IDA exhibited the lowest semicircle (fast charge transfer) and highest line (fast electron diffusion) compared with IDA and N-CNS electrodes. These data support the CV data of fast charge transfer and efficient catalytic activity due to the high electron diffusion and low surface resistance on the surface of N-CNB/IDA. These results provide the functional design of chipset electrode based on N-CNB with novel surface topography of nanobuds aligned at the electrode, including the carbon surface, meso–microporous network, surface defects/free spaces, and functionalized surface of N-doped carbon chain, the formation of numerous plane edge defects, and surface polarization with a pool of electrons.

The sensing property of the chipset nanosensor of N-CNB/IDA for EP detection was examined using CV in 0.1 M phosphate buffer (PB) (pH=7). Figure 3C shows the CVs of 100 µM EP on

IDA (a), N-CNS/IDA (b), and N-CNB/IDA (c). N-CNB/IDA showed four strong defined peaks centered at 0.33, 0.26, -0.026, and -0.063 V. Four peaks with low peak current intensities and varied applied potential peak positions were also recorded using the IDA and N-CNS/IDA. The four peaks were related to the oxidation of EP that results in the formation of quinone (I), reduction of quinone (peak II), oxidation of leucoadrenochrome to adrenochrome (III), and reduction of a cyclized product from adrenochrome to leucoadrenochrome (IV) [29]. The N-CNB/IDA showed a high sensing property for EP detection due to the surface morphology, high surface area, low surface charge resistance, functionalized surface with strong binding to EP molecules, and facile electron/molecular diffusion of the nanobuds [11c, 30]. The sensitivity of N-CNB/IDA for EP detection was confirmed by screening of various EP concentrations (0, 100, and 200 µM) using CV technique (Figure 3D). The four oxidation–reduction peaks of EP increased with the increase in EP concentrations.

Selectivity is one of the important factors that influence the affinity and quality of the designed sensors. Electrochemical signaling of EP is affected by the presence of ascorbic acid (AA) and UA. Electrochemical signaling of AA, EP, and UA in one-run may overlap in one broad peak using the bare electrodes [5b, 12d, 31]. So, we tested the selectivity of EP sensor in the presence of these potentially interfering molecules and other metal ions that may presents in the real human serum. Figure 3E shows the screening of 500 µM AA and 100 µM EP using CV technique on N-CNB/IDA. Two well-defined peaks were observed at an applied potential of 0.13 and 0.33 V for AA and EP, respectively, leading to the selective monitoring of EP in the presence of high concentrations of AA. Figure 3F shows the screening of AA (500 µM), EP (100 µM), K^+ (500 µM), Na^+ (500 µM), Ca^{2+} (500 µM), and UA (100 µM). Three well-defined peaks were obtained and centered at 0.13, 0.33, and 0.42 V for AA, EP, and UA, respectively. However, no response was observed for the other interfering ions. These results enabled the design of a highly selective chipset nanosensor based on N-CNB for the screening of EP in the presence of potential interfering molecules and cations. Therefore, N-CNB/IDA can be used as a sensitive

and selective portable EP sensor. The designed chipset nanosensor based on N-CNB/IDA conveyed the advantages of a) strong signaling of EP, b) high signaling at low sample volume, and c) stable sensing property at high and low concentrations of EP. The N-CNB natural surface morphology and chemical composition offered the advantages of a) high S_{BET}, b) meso–microporous construction, c) novel morphology of nanobuds, free spaces, heterogeneous surface alignment, and weaved surface with rough texture, d) N doping of the sp^2 carbon network, e) formation of multiple active centers with numerous plane edge defects, f) heavy EP binding to the surface of N-CNB/IDA, and g) rapid charge transport with a low surface resistance [11c, 26a, 26b, 30].

Figure 3

2.2 Physicochemical parameters for sensing performance and surface interaction of EP on N-CNB/IDA

The pH dependence of the supporting electrolyte and the effects of scan rate were studied to investigate the optimum sensing performance and illustrate the related physicochemical parameters. The scan rate effect (20–280 mVs^{-1}) during the sensing of EP (50 µM) was determined on N-CNB/IDA using CV in the range of -0.2 V to +0.8 V and fixed pH of 7 (Figure 4A). With the increase in the scan rate, the current peak values increased (four EP peaks) with a small and gradually applied potential shift (E/V) to positive values. This behavior confirms the scan rate effect on EP sensing performance and indicates the actual surface interaction of EP and N-CNB (a controlled adsorption process). The plot of anodic (Ia) and cathodic (Ic) current values versus the scan rate (mVs^{-1}) indicated a linear relationship with the regression equations of Ia (µA) = 1.8 + 0.02 ν (mVs^{-1}), R^2 = 0.986 and Ic (µA) = –0.2 – 0.01 ν (mVs^{-1}), R^2 = 0.0.99 (S/N = 3) (Figure 4B). The linear relationship of scan rate versus current peak values and the position shift of E/V with the increase in scan rate indicates that the adsorption-controlled process was the main mechanism of surface interaction between EP and N-CNB/IDA

[11c, 26a, 30]. The amount of EP molecules adsorbed on the surface of N-NCB/IDA can be calculated by applying the following equation [32]:

$$I_a = n^2F^2\Gamma\nu A/4RT, \quad (1)$$

where A represents the IDA surface area, R is the gas constant, Γ denotes the number of adsorbed molecules, n refers to the number of electrons transferred, F is Faraday's constant, T indicates the absolute temperature, and ν stands for the scan rate. The calculated adsorbed EP molecules on the surface of N-CNB/IDA reached 2.8×10^{-9} mole/cm^2.

The electron transfer rate constant (Ks) and charge transfer coefficient (α) of the redox interaction of EP on the surface of N-CNB/IDA were calculated by applying Laviron's theory [33].

Figure 4C shows the plot of Log ν versus Ea and Ec. The relationships between log ν and Ea and Ec values were linear, and the equations were Ea (V) = 0.39 + 0.007 log ν (V s^{-1}) (R^2 = 0.968) and Ec(V) = 0.19 – 0.036 log ν (V s^{-1}) (R^2 = 0.999).

By applying the following equations, α and Ks were calculated to be 0.23 s and 0.11 cms^{-1}, respectively.

$$\log k_a/k_c = \log \alpha/(1-\alpha) \text{ or } k_a/k_c = \alpha/(1-\alpha) \quad (2)$$

$$\boldsymbol{logKs = \alpha\log(1-\alpha) + (1-\alpha)\log\alpha - \log\frac{RT}{nF\nu} - \frac{\alpha(1-\alpha)nF\Delta Ep}{2.3RT}} \quad (3)$$

where Ka (slope of Ea vs. log ν) equals 2.3RT/(1 − α) nF, and Kc (slope of Ec vs. log ν) equals −2.3RT/αnF.

The pH of the supporting electrolyte is one of the important factors for EP signaling in biological samples. The pH-dependent effect on the EP sensing property was studied by signaling 100 µM EP using CV under various pH (5–8) and a scan rate of 100 mVs^{-1} (Figure 4D). The Ia and Ic peak current values varied with the change in pH, and a high current value was observed at pH = 7 (Figure 4E). In addition, the E/V values negatively shifted with the increase in pH and showed a linear relationship between pH and E/V with the regression

equation of E/V = 0.64–0.059 pH (R^2 = 0.981) (Figure 4F). This behavior and the slope value ascertained the proton participation in the overall process with the suggested mechanism of $\pm 2e^-/2H^+$ [11a, 11c, 12b]. In conclusion, the electrooxidation of EP on the N-CNB/IDA surface occurred with fast charge transfer, high target loading, and strong binding to the target molecules (adsorption-controlled process mechanism).

Figure 4

2.3 Sensitivity, stability, and reusability of the chipset nanosensor N-CNB/IDA for quantification of EP

The sensitivity, stability, and reproducibility of the chipset nanosensor of N-CNB/IDA for EP monitoring were studied using various electrochemical techniques, including SWV and chronoamperometry (CA). Figure 5A shows the photographs of the chipset nanosensor used to design a portable biosensor-based device. The chipset IDA was in direct contact with the potentiostat through a cable. The cable transferred the signaling data of the EP electrooxidation process to the surface of N-CNB/IDA. The volume needed to read out the test (EP samples) was extremely low (10 µL) (Figure 5Ab). The designed chipset nanosensor sensitivity was tested using SWV under various EP concentrations (0.5–140 µM) (Figure 5B). With the increase in EP concentrations, the anodic current peak increased. At high EP concentrations, the current response decreased to a low concentration due to the electrode surface saturation by EP molecules (adsorption-controlled process) (Figure 5Ca). The inset in Figure 4B exhibits the dramatic sensitive response obtained by the increased concentrations from 0.5 to 3 µM. The plot of EP concentrations (µM) and the response peak current (µA) revealed a linear relationship with the equation of I (µA) = 5.9 + 4.74 [Ep](µM), R^2 = 0.991 (S/N = 3) within the range of 0.5–3 µM (Figure 5Cb). Based on the linear equation (3σ/slope, σ is the standard error of the intercept), the detection limit was 0.022 µM.

The stable and sensitive response was confirmed using another sensitive electrochemical technique (CA) at a fixed applied potential of 0.33 V. Figure 5D shows the CA response upon

the successive addition of EP concentrations from 0.2 to 135 µM (Figure 5D and its inset). A sensitive and gradual increase in the CA current response was observed with the increase in EP concentrations. The sensitive and stable response verified the sensitivity of the portable sensor based on N-CNB/IDA for EP detection. Figures 5E(a and b) show the calibration plot of [EP]/µM versus the anodic current response (µA). A linear relationship was obtained with the equation of I (µA) = 0.34 + 0.003 [EP](µM), R^2 = 0.98 (S/N = 3) for the concentration range of 0.2–1 µM (Figure 5Eb). The detection limit was 0.011 µM. These data revealed the successful design of a highly sensitive EP chipset nanosensor using N-NCB/IDA. The surface morphology, nature, and chemical composition played key roles in the sensitive and selective assay for EP monitoring. N-CNB/IDA illustrated a highly sensitive EP sensor with a low detection limit and wide linear range compared with the other designed electrodes (Table S2). The N-CNB/IDA exhibited fast response (~10 s), high stability, high economy, portable EP sensors, low sample volume, and high sensitivity and selectivity.

The stability and reproducibility of chipset EP nanosensor assay based on N-CNB/IDA were examined by SWV using various electrodes and samples. A stable response was observed when detecting six EP samples (0.5 µM) with % relative standard deviation (RSD) of 1.46 and a standard deviation (SDEV) of ±0.04 µM (Figure S2A). The N-CNB/IDA shows a good reproducibility even after using various designed sensors (five chipset N-CNB/IDA). A stable and sensitive EP (0.3 µM) signaling using five chipset N-CNB/IDA was indicated with %RSD = 2.7 and SDEV = ±0.05 (Figure S2B). These data reveal the successful design of a highly stable, sensitive, selective, and reproducible chipset nanosensor based on N-CNB/IDA for the detection of EP.

Figure 5

2.4 Monitoring of EP in human serum using the chipset nanosensor based on N-CNB/IDA

The analytical and clinical investigation of several neurological disorders can be followed up by detecting neurotransmitters (i.e., EP) in complex media (i.e., human serum). In this analysis,

the serum solution was prepared by adding 100 µL human serum sample to 10 mL PB (pH=7). Using the SWV technique, the N-CNB/IDA chipset nanosensor was used for screening of various concentrations of EP (0.5–2.5 µM) (Table 1). The N-CNB/IDA showed a high EP recovery (97.2 % – 99.28 %) in the human serum samples. These findings indicate that N-CNB/IDA is adequate for the selective screening of EP in human serum samples. Therefore, the sensory EP protocol based on chipset design of a nanosensor based on N-CNB/IDA can be used to develop a promising portable biosensor and economical analytical method for clinical applications with rapid response, high sensitivity, and good selectivity.

Scheme 2 describes the chipset nanosensor of N-CNB/IDA with multiple functionalized active sites used for the detection of EP molecules. The N-CNB materials can transfer signaling with high speed due to the formation of an active surface with a pool of electrons and high loading and migratory movements of EP molecules on the inner/outer N-CNB surface. The N atoms doped the carbon chain and created multi-functional active centers with numerous plane edge defects and high electron density. Moreover, high surface area, microporous network, rough surface texture, free groove spaces, and surface heterogeneity of nanobuds grown on the electrode surface induced the mobility of EP molecules and enlarged the surface interface area. Therefore, the selective signaling of EP on the chipset nanosensor of N-CNB/IDA was accomplished with extremely high sensitivity and stability due to the strong binding to EP molecules, facile electron/molecular diffusion, and fast charge transfer. The chipset nanosensor of N-CNB/IDA can be used as a portable EP sensor in clinical trials of related functions, including neurological disorders, and in intensive care units.

Scheme 2

Table 1

3. Conclusion

Portable devices for healthcare applications can be designed based on the nanofabrication of chipset array electrodes. Here, we functionalized a chipset nanosensor of IDA by N-doped carbon materials. N-CNB and N-CNS were synthesized using a simple approach and low-cost organic procedures. The chipset nanosensor was assembled based on modification of the active IDA surface by N-CNB and N-CNS. The sensing property and catalytic activity of key components depend on the surface heterogeneity formation and chemical composition of N-CNB. The surface heterogeneity of N-CNB was obtained from the irregular growth of nanobuds in vertical and horizontal directions and various lengths and sizes (size range: 70–150 nm). The surface functionality (the presence of N-functionality) and foundation of free spaces, such as heterogeneous angularities and V-shaped spaces, facilitated the solid–liquid interface electrolyte contact and diffusion. These intrinsic features led to the production of low-cost carbon-based materials with multi-functional active centers and a charged surface rich in electrons. N-CNB/IDA was used to develop a highly sensitive and selective chipset nanosensor for screening of EP level in human fluids. Therefore, the designed sensor based on N-CNB/IDA provides fast signaling, sensitive and selective monitoring, low detection limit, wide linear range, and on-site detection. A portable sensor can be designed based on N-CNB/IDA for on-site EP detection in human serum samples and could be matched with portable smartphones as a power source and signaling reader.

4. Experimental Section/Methods

4.1 Fabrication of N-CNB and N -doped carbon nanoparticles (N-CNS) on IDA.

The controlled synthesis of N-CNB and N-CNS was performed using hydrothermal treatment (HT) of hydrocarbons (i.e., glucose) at elevated temperatures [11c].

1- For the synthesis of N-CNB, a) a glucose solution (carbon source) was prepared by dissolving 1.8 g glucose (0.2 M) in 30 mL Milli-Q water, and the resulting mixture was stirred

for 2 h (solution a). b) Pluronic F127 (0.5 g) was dissolved in solution (a) by continuous stirring until a homogeneous solution was obtained. c) The uric acid (UA) solution (solution b) (nitrogen source) was prepared by dispersing 0.5 g UA in 0.1 M NaOH (20 mL); the mixture was sonicated for 1 h and then stir red for 2 h. Both solutions (a and b) were mixed and stirred for 1 h at room temperature (solution A).

2- For N-CNS, a) the glucose solution was prepared following steps a and b. b) The 4-amino benzoic acid solution was prepared by dissolving 0.5 g in 20 mL 0.1 M NaOH. c) The glucose and 4-aminobenzoic acid solutions were mixed and then stirred for 2 h (solution B).

3- Solutions A and B were poured into 100 mL Teflon-sealed autoclaves and stored at 180 °C for 24 h. The black precipitates of N-CNB and N-CNS were collected after cooling to room temperature. The precipitates were washed several times with a 1:1 water/ethanol solution before being dried at 80 °C for 24 h. Under N_2 atmosphere, the prepared N-CNB and N-CNS materials were annealed at 800 °C for 2 h with a 3 °C/min temperature phase rise.

4.2 Fabrication of portable sensor based on N-CNB/IDA and N-CNS/IDA.

A portable and chipset nanosensor was designed based on the fabrication of N-CNB and N-CNS on the IDA electrode. The fabrication process was performed as follows: a) The ink formation of N-CNB and N-CNS was prepared by dispersing of 10 mg of each sample in 1 mL deionized water (sonicated for 3 h). b) The IDAs were fabricated by drop-casting 20 µL N-CNB and N-CNS ink solutions to the open IDA electrode area. The portable and chipset electrodes were named as N-CNB/IDA and N-CNS/IDA, respectively. c) The reference electrode for the IDA electrode was fabricated by adding Ag/AgCl ink and heating at 80 °C for 1 min to form a thin-film layer of Ag/AgCl. d) The designed electrodes were stabilized for 10 cycles using continuous cyclic voltammetry sweeps in 0.1 M PB (pH = 7) at a scan rate of 100 mVs^{-1} within the potential window of 0.0–1.6 V.

4.3 EP level tracking in human blood serum using chipset N-CNB/IDA.

The actual monitoring of EP was examined using the standard additive method in a human serum sample. The serum solution sample was prepared by mixing 10 µL serum samples with 10 mL PB (pH 7). Then, various standard solutions of EP were added to the human serum sample solution. Afterward, 10 µL solution sample was added to the working area of N-CNB/IDA. EP was measured using square wave voltammetry (SWV) technique at 20 Hz frequency, 0.5 V step height, 10 mV step amplitude, and 3 ms time integration.

Supporting Information (1. Experimental section containing Materials, Electrochemical sensing system, and Characterization analyses; The NLDFT, Raman, and XPS analysis of N-CNS and N-CNB materials; stability performance; and table of comparison of various electrode materials for EP detection) Supporting Information is available from the Wiley Online Library.

Acknowledgements

This work was supported by the Japan Society for the Promotion of Science (JSPS), grant No. P19067.

References

[1] C. Dincer, R. Bruch, E. Costa-Rama, M. T. Fernández-Abedul, A. Merkoçi, A. Manz, G. A. Urban, F. Güder, *Adv.Mater.***2019**, 31, 1806739.

[2] a) A. Hourlier-Fargette, S. Schon, Y. Xue, R. Avila, W. Li, Y. Gao, C. Liu, S. B. Kim, M. S. Raj, K. B. Fields, B. V. Parsons, K. Lee, J. Y. Lee, H. U. Chung, S. P. Lee, M. Johnson, A. J. Bandodkar, P. Gutruf, J. B. Model, A. J. Aranyosi, J. Choi, T. R. Ray, R. Ghaffari, Y. Huang, J. A. Rogers, *Lab on a Chip* **2020**, 20, 4391; b) F. Sassa, G. C. Biswas, H. Suzuki, *Lab on a Chip* **2020**, 20, 1358; c) S. A. El-Safty, M. A. Shenashen, *Adv.Mater. Interfaces* **2020**, 7, 2000153; d) S. A. El-Safty, M. A. Shenashen, *Mater.Tod. Bio* **2020**, 5, 100044.

[3] a) A. Reda, S. A. El-Safty, M. M. Selim, M. A. Shenashen, *Biosens.Bioelectron.* **2021**, 185, 113237; b) M. A. Shenashen, M. Y. Emran, A. El Sabagh, M. M. Selim, A. Elmarakbi, S. A. El-Safty, *Prog. Mater. Sci.* **2021**, DOI: https://doi.org/10.1016/j.pmatsci.2021.100866100866.

[4] a) J. Lee, D. Sharma, Y. Lim, H. Shin, *Sens. Actuators B: Chem.* **2018**, 267, 467; b) R. D. Abdel-Rahim, M. Y. Emran, A. M. Nagiub, O. A. Farghaly, M. A. Taher, *Electroch. Sci. Adv.* **2021**, 1, e2000031.

[5] a) S. Feng, Y. Li, R. Zhang, Y. Li, *Biosens. Bioelectron.* **2019**, 142, 111491; b) Y. Hu, Y. He, Z. Peng, Y. Li, *Biosens. Bioelectron.* **2020**, 167, 112490; c) J. Yang, Y. Hu, Y. Li, *Biosens. Bioelectron.* **2019**, 135, 224.

[6] a) M. B. Joseph, E. Bitziou, T. L. Read, L. Meng, N. L. Palmer, T. P. Mollart, M. E. Newton, J. V. Macpherson, *Anal. Chem.* **2014**, 86, 5238; b) M. Bariya, Z. Shahpar, H. Park, J. Sun, Y. Jung, W. Gao, H. Y. Y. Nyein, T. S. Liaw, L.-C. Tai, Q. P. Ngo, *ACS Nano* **2018**, 12, 6978; c) M. Song, L. Dang, J. Long, C. Hu, *ACS Sensors* **2018**, 3, 2518; d) M. Sun, T. Xin, Z. Ran, X. Pei, C. Ma, J. Liu, M. Cao, J. Bai, M. Zhou, *ACS Sensors* **2021**, 6, 275.

[7] a) S. K. Arya, G. Chornokur, M. Venugopal, S. Bhansali, *Analyst* **2010**, 135, 1941; b) K. V. Singh, D. K. Bhura, G. Nandamuri, A. M. Whited, D. Evans, J. King, R. Solanki, *Langmuir* **2011**, 27, 13931.

[8] C. E. Nwankire, A. Venkatanarayanan, T. Glennon, T. E. Keyes, R. J. Forster, J. Ducree, *Biosens. Bioelectron.* **2015**, 68, 382.

[9] T. Li, Y. Fan, Y. Cheng, J. Yang, *Lab on a Chip* **2013**, 13, 2634.

[10] a) Z. Li, Y. Guo, H. Yue, X. Gao, S. Huang, X. Zhang, Y. Yu, H. Zhang, H. Zhang, *J. Electroanal. Chem.* **2021**, 895, 115425; b) K. Chetankumar, B. E. K. Swamy, H. S. B. Naik, *Mater.Chem. Phys.* **2021**, 267, 124610; c) W. Zhang, G. Jia, Z. Li, C. Yuan, Y. Bai, D. Fu, *Adv. Mater. Interfaces* **2017**, 4, 1601241; d) Q. Huang, X. Lin, L. Tong, Q.-X. Tong, *ACS Sust. Chem. Eng.* **2020**, 8, 1644; e) J. Li, H. Shen, S. Yu, G. Zhang, C. Ren, X. Hu, Z. Yang, *Analyst* **2020**, 145, 3283.

[11] a) M. Y. Emran, S. A. El-Safty, M. M. Selim, A. Reda, H. Morita, M. A. Shenashen, *Carbon* **2021**, 173, 1093; b) M. Y. Emran, S. A. El-Safty, M. A. Shenashen, T. Minowa, *Sens. Actuators B: Chem.* **2019**, 284, 456; c) M. Y. Emran, M. A. Shenashen, A. A. Abdelwahab, M. Abdelmottaleb, S. A. El-Safty, *New J. Chem.* **2018**, 42, 5037; d) H. S. Hwang, J. W. Jeong, Y. A. Kim, M. Chang, *Micromachines* **2020**, 11, 814.

[12] a) M. Y. Emran, S. A. El-Safty, M. M. Selim, M. A. Shenashen, *Sens. Actuators B: Chem.* **2021**, 329, 129192; b) M. Y. Emran, S. A. El-Safty, M. M. Selim, T. Minowa, A. Elmarakbi, M. A. Shenashen, *Anal. Chim. Acta* **2021**, 1142, 143; c) M. Y. Emran, M. A. Shenashen, S. A. El-Safty, M. M. Selim, T. Minowa, A. Elmarakbi, *ACS Appl. Biomater.***2020**, 3, 8496; d) A. A. Abdelwahab, A. H. Naggar, M. Abdelmotaleb, M. Y. Emran, *Electroanalysis* **2020,** 32 (10), 2156-2165; e) N. Akhtar, S. A. El-Safty, M. E. Abdelsalam, H. Kawarada, *Adv. Healthcare Mater.* **2015**, 4, 2110; f) B. Huang, X. Hu, Y. Liu, W. Qi, Z. Xie, *J. Power Sour.* **2019**, 413, 408; g) M. Y. Emran, E. Talat,

S. El-Safty, M. Shenashen, E. Saad, *New J. Chem.*, ***2021***,45, 5452-5462; h) F. Zhang, M. Li, H. Li, G. Wang, Y. Long, P. Li, C. Li, B. Yang, *Carbon* **2021**, 175, 364.

[13] a) G. Azuara-Tuexi, J. A. Méndez-Cabañas, E. Muñoz-Sandoval, R. A. Guirado-López, *Carbon* **2021**, 175, 387; b) J. Su, Y. Zhao, J. Xi, *Electrochim. Acta* **2018**, 286, 22; c) A. S. Galushko, E. G. Gordeev, V. P. Ananikov, *Langmuir* **2018**, 34, 15739.

[14] a) Z. Jemelkova, J. Barek, J. Zima, *Anal. Lett.* **2010**, 43, 1367; b) Y. Sun, Y. Wang, Y. Yang, M. Yang, *Chem. Lett.* **2018**, 48, 215; c) M. Y. Emran, H. Khalifa, H. Gomaa, M. A. Shenashen, N. Akhtar, M. Mekawy, A. Faheem, S. A. El-Safty, *Microchim. Acta* **2017**, 184, 4553; d) M. Y. Emran, M. A. Shenashen, M. Mekawy, A. M. Azzam, N. Akhtar, H. Gomaa, M. M. Selim, A. Faheem, S. A. El-Safty, *Sens. Actuators B: Chem.* **2018**, 259, 114.

[15] F. Rémy, F. Mirrashed, B. Campbell, W. Richter, *Neuroimage* **2005**, 25, 253.

[16] a) H. Takano, *Front Psychiatry* **2018**, 9, 228; b) K. Chen, O. Cases, I. Rebrin, W. Wu, T. K. Gallaher, I. Seif, J. C. Shih, *J. Biological Chem.* **2007**, 282, 115; c) H. M. M. Asjad, A. Kasture, A. El-Kasaby, M. Sackel, T. Hummel, M. Freissmuth, S. Sucic, *J. Biological Chem.* **2017**, 292, 19250.

[17] a) X.-E. Zhao, Y.-R. Suo, *Talanta* **2008**, 76, 690; b) A. S. Moody, B. Sharma, *ACS Chem. Neurosc.* **2018**, 9, 1380; c) Y. Zhang, W. Ren, Y. Z. Fan, J. X. Dong, H. Zhang, H. Q. Luo, N. B. Li, *Anal. Chim. Acta* **2019**, 1054, 167; d) J. Du, L. Shen, J. Lu, *Anal. Chim. Acta* **2003**, 489, 183; e) T. Li, Z. Wang, H. Xie, Z. Fu, *J. Chromatog. B* **2012**, 911, 1.

[18] A. G. Nasibulin, P. V. Pikhitsa, H. Jiang, D. P. Brown, A. V. Krasheninnikov, A. S. Anisimov, P. Queipo, A. Moisala, D. Gonzalez, G. Lientschnig, *Nat. Nanotechn.* **2007**, 2, 156.

[19] a) Q. Wang, H. Li, L. Chen, X. Huang, *Solid State Ionics* **2002**, 152, 43; b) M.-M. Titirici, M. Antonietti, N. Baccile, *Green Chem.* **2008**, 10, 1204.

[20] a) S. N. Faisal, E. Haque, N. Noorbehesht, W. Zhang, A. T. Harris, T. L. Church, A. I. Minett, *RSC Adv.* **2017**, 7, 17950; b) E. Haque, M. M. Islam, E. Pourazadi, M. Hassan, S. N. Faisal, A. K. Roy, K. Konstantinov, A. T. Harris, A. I. Minett, V. G. Gomes, *RSC Adv.* **2015**, 5, 30679; c) Y. Zou, W. Zhong, S. Li, J. Luo, C. Xiong, W. Yang, *Electrochim. Acta* **2016**, 212, 828; d) M. Islam, S. N. Faisal, A. K. Roy, S. Ansari, D. Cardillo, K. K. Konstantinov, E. Haque, *J. Nanotechnol. Mater. Sci.* **2015**, 2(1), 1–5.

[21] K. Parvez, S. Yang, Y. Hernandez, A. Winter, A. Turchanin, X. Feng, K. Müllen, *ACS Nano* **2012**, 6, 9541.

[22] a) J. Wei, Y. Liang, X. Zhang, G. P. Simon, D. Zhao, J. Zhang, S. Jiang, H. Wang, *Nanoscale* **2015**, 7, 6247; b) Y.-s. Jung, W. Park, H. Park, D.-K. Lee, K. Na, *Carbohydrate polymers* **2017**, 156, 403.

[23] a) S. A. El-Safty, M. Khairy, M. A. Shenashen, E. Elshehy, W. Warkocki, M. Sakai, *Nano Res.* **2015**, 8, 3150; b) M. A. Shenashen, N. Akhtar, M. M. Selim, W. M. Morsy, H. Yamaguchi, S. Kawada, A. A. Alhamid, N. Ohashi, I. Ichinose, S. A. El-Safty, *Chem. Asian J.* **2017**, 12, 1952.

[24] M. Pimenta, G. Dresselhaus, M. S. Dresselhaus, L. Cancado, A. Jorio, R. Saito, *Phy. Chem. Chem. Phys.* **2007**, 9, 1276.

[25] a) N. Akhtar, S. A. El-Safty, M. Khairy, W. A. El-Said, *Sens.Actuators B: Chem.* **2015**, 207, 158; b) M. A. Shenashen, D. Hassen, S. A. El-Safty, M. M. Selim, N. Akhtar, A. Chatterjee, A. Elmarakbi, *Adv.Mater.Interfaces* **2016**, 3, 1600743.

[26] a) M. Y. Emran, M. A. Shenashen, H. Morita, S. A. El-Safty, *Adv. Healthcare Mater.* **2018**, 7, 1701459; b) M. Y. Emran, M. Mekawy, N. Akhtar, M. A. Shenashen, I. M. EL-Sewify, A. Faheem, S. A. El-Safty, *Biosen. Bioelectron.* **2018**, 100, 122; c) Z. Li, F. Bu, J. Wei, W. Yao, L. Wang, Z. Chen, D. Pan, M. Wu, *Nanoscale* **2018**, 10, 22871.

[27] a) N. Akhtar, S. A. El-Safty, M. E. Abdelsalam, M. A. Shenashen, H. Kawarada, *Biosens. Bioelectron.* **2016**, 77, 656; b) N. Akhtar, M. Y. Emran, M. Shenashen, H. Khalifa, T. Osaka, A. Faheem, T. Homma, H. Kawarada, S. El-Safty, *J. Mater. Chem. B* **2017**, 5, 7985-7996.

[28] D. Buttry, A. Bard, Marcel Dekker, New York, 1991.

[29] a) J. Y. Bai, L. Wang, H. J. Wang, P. F. Huang, Y. Q. Zhao, S. Di Fan, *Microchim. Acta* **2006**, 156, 321; b) S.-f. Wang, D. Du, Q.-C. Zou, *Talanta* **2002**, 57, 687.

[30] M. Y. Emran, M. A. Shenashen, H. Morita, S. A. El-Safty, *Biosens. Bioelectron.* **2018**, 109, 237.

[31] K. Barman, S. Jasimuddin, *RSC Adv.* **2016**, 6, 99983.

[32] M. Sharp, M. Petersson, K. Edström, *J. Electroanal.Chem. Interfacial Electrochem.* **1979**, 95, 123.

[33] E. Laviron, *J. Electroanal.Chem. Interfacial Electrochem.* **1979**, 101, 19.

Figures

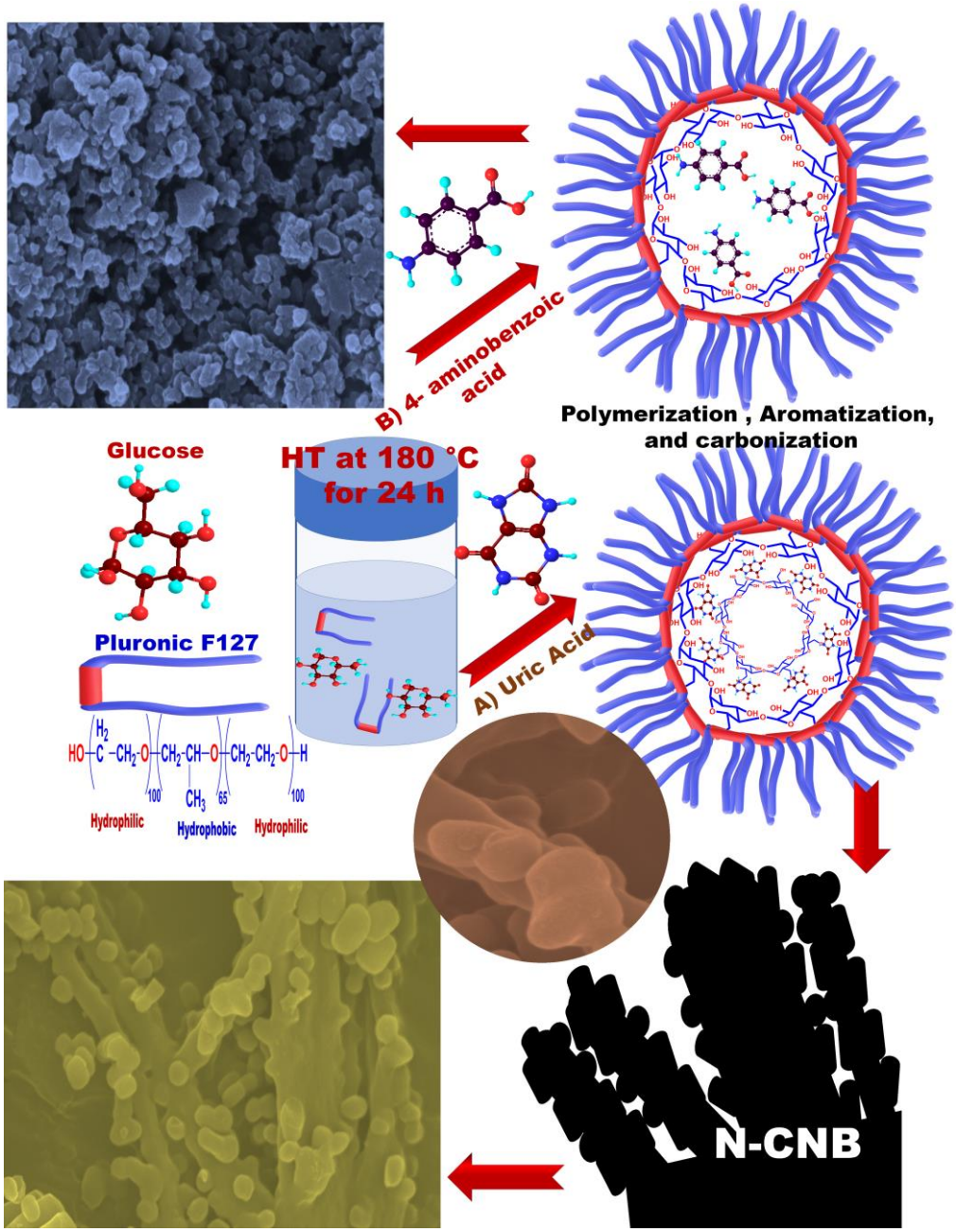

Scheme 1. The Schematic diagram for control synthesis of N doped carbon nanobuds (N-CNB) and N-doped carbon nanostructures (N-CNS). A) The controlled formation of N-CNB after thermal treating of uric acid and glucose in the presence of F127 as directing agent. B) The controlled formation of N-CNB after thermal treating of p-aminobenzoic acid and glucose in the presence of F127 as directing agent.

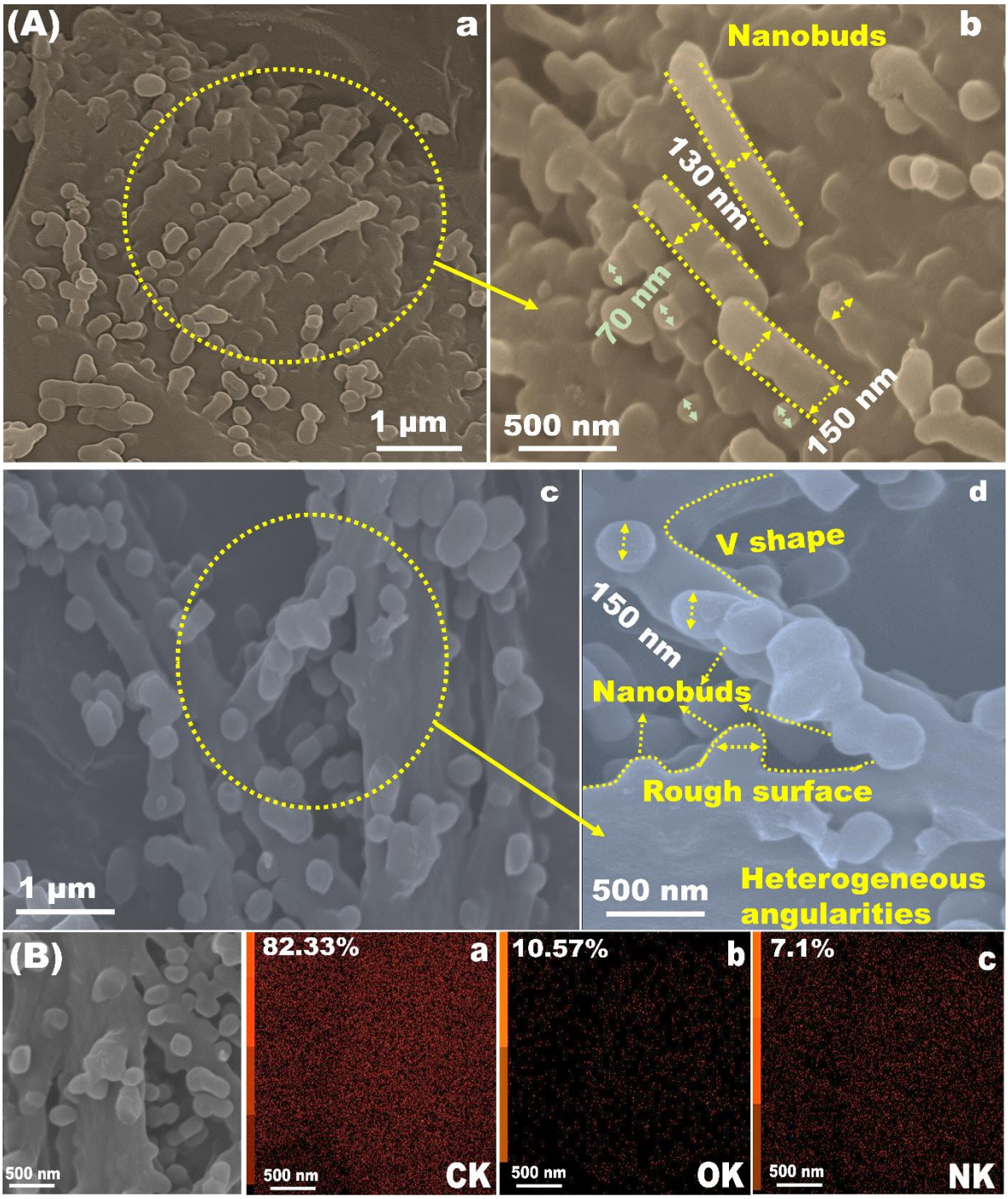

Figure 1. A) The FE-SEM images of N-CNB at various positions and magnifications (a-d). B(The EDS-SEM mapping of N-CNB for C K (a), O K (b) , and N k (c).

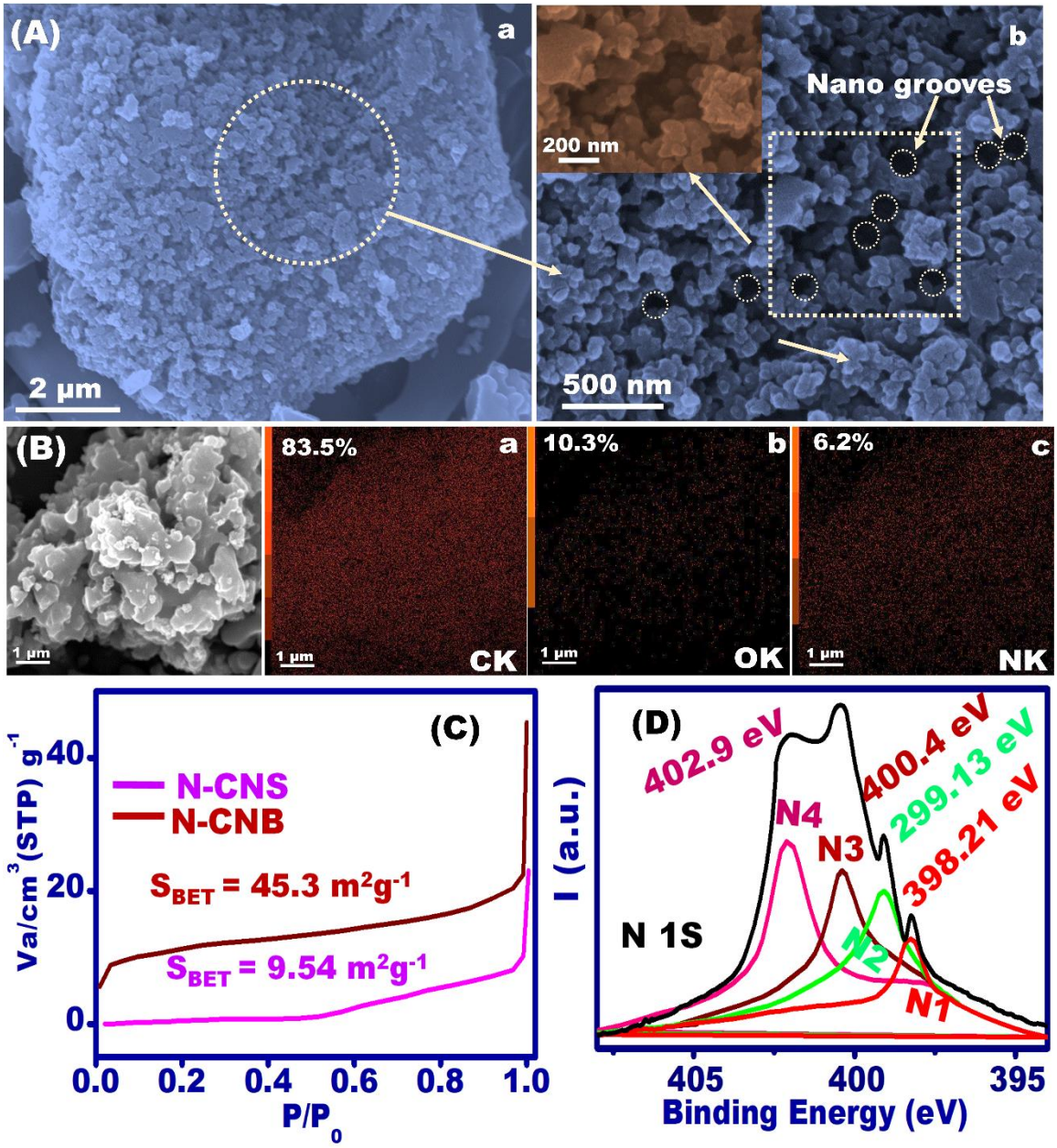

Figure 2. A) The FE-SEM images of N-CNS at loe magnification (a), high magnification (b). The inset of b) shows the high magnification FE-SEM image focused on the grooves and vacant area at the surface sutructure. B) The EDS-SEM mapping of N-CNS for C K (a), O K (b) , and N k (c). C) The N_2 adsorption isotherm of N-CNB (wine line), and N-CNS (ponk line). D) The XPS servey of N 1s of N-CNB **.**

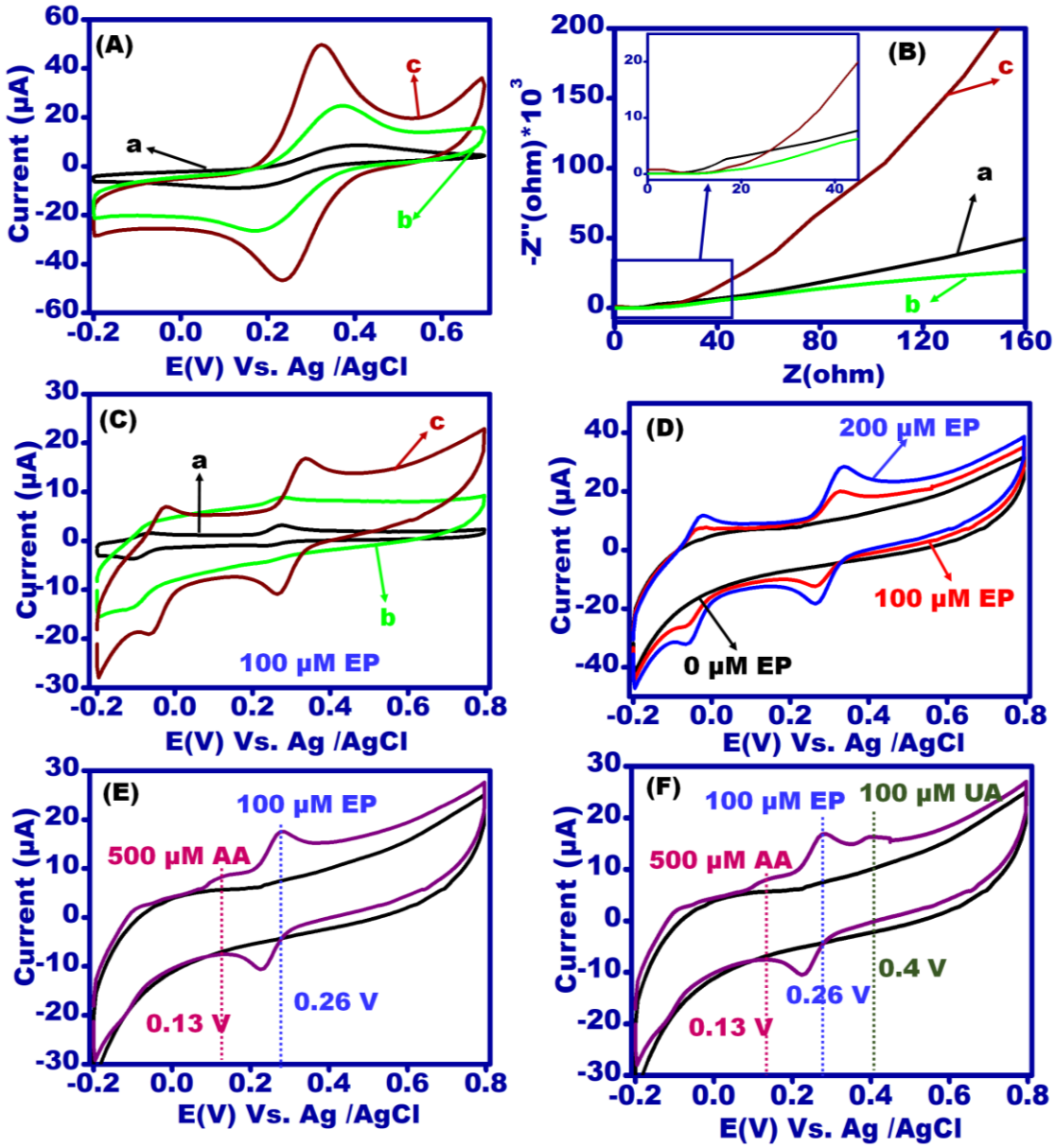

Figure 3. A) The CVs of IDA (a), N-CNS/IDA (b), and N-CNB/IDA (c) in 0.1 M KCl containing 5 mM $[Fe(CN)_6]^{3-/4-}$ at scan rate of 100 mVs^{-1}. B) The EIS Nyquist plot of IDA (a), N-CNS/IDA (b), and N-CNB/IDA (c) in 0.1 M KCl containing 5 mM $[Fe(CN)_6]^{3-/4-}$. Inset of B) The focused EIS measurements at small area for illustrating the semicircle and diffusion line of the various electrodes. C) The CVs of IDA (a), N-CNS/IDA (b), and N-CNB/IDA (c) in 100 μM EP (PB, pH = 7). D) The CVs of various EP-concentrations of 0, 100, and 200 μM (PB, pH = 7) on N-doped N-CNB/IDA. E) The CVs of 0 M (black line) and 500 AA μM+ 100 μM EP (violet line) on N-CNB/IDA. F) The CVs of 0 M (black line) and 500 AA μM+ 100 μM NA+100 μM UA (violet line) on N-CNB/IDA.

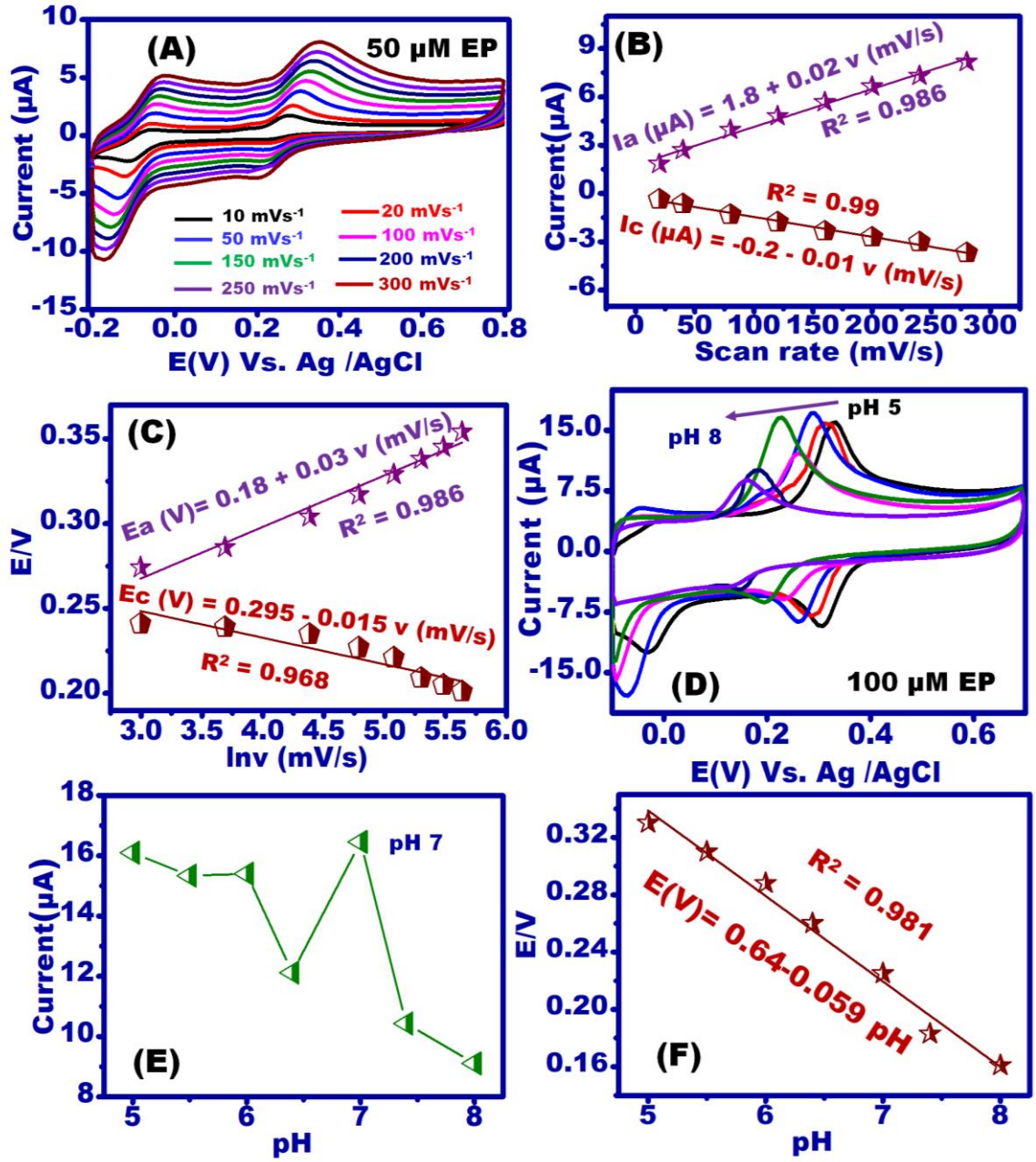

Figure 4. A) The CVs of 50 µM EP at various scan rate from 20 – 300 mvs-1 in 0.1 M PB (pH 7) on N-CNB/IDA. B) The plot of scan rate (mVs^{-1}) Vs anodic (Ia), and cathodic (Ic) currents (µA). C) the plot of log scan rate (V/s) Vs the anodic (Ea) and cathodic (Ec) applied potential (E/V). D) The CVs of 100 µM EP within varying the pH value (5 –8). The plot of pH Vs the anodic current (E) and anodic applied potential (F).

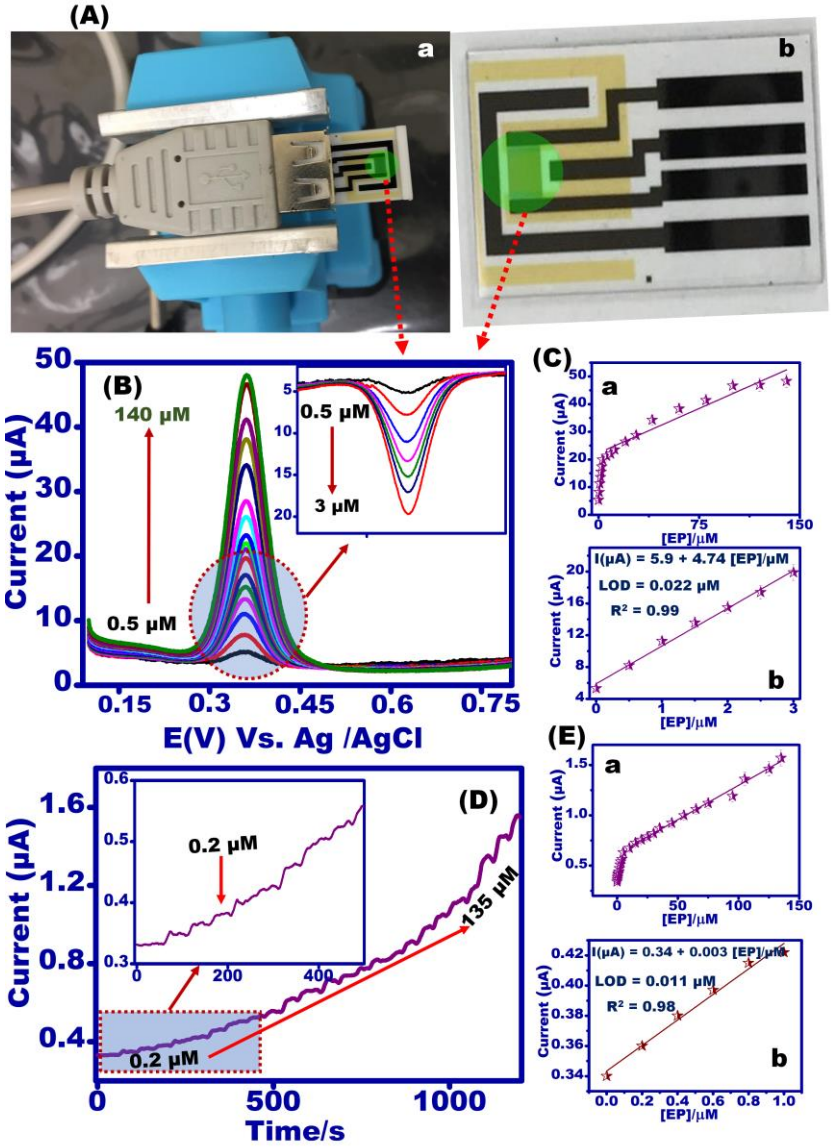

Figure 5. A) The photo images of chipset design of IDA that used as a portable electrode for signaling of EP in human fluids. B) The SWV measurements of various EP concentrations in the range of 0.5 –140 µM on N-CNB/IDA. Inset of B) The SWV-measurements at low concentrations from 0.5 – 3 µM. Ca) The calibration plot of [EP]/(µM) Vs the current (µA) at wide range of 0.5 – 140 µM. Cb) The calibration plot of [EP]/(µM) Vs the current (µA) at wide range of 0.5 – 3 µM. D) The chronoamperometry (CA) response of EP within dynamic injection of various concentrations from 0.2 to 135 µM at fixed applied potential of 0.33 V, under continuous stirring and N_2 flow. Ea) The calibration plot of [DA]/(µM) Vs the current (µA) at wide range of 0.2 – 135 µM. Inset of D shows the CA response at low concentrations. Eb) the calibration plot in the range of 0.2 – 1 µM.

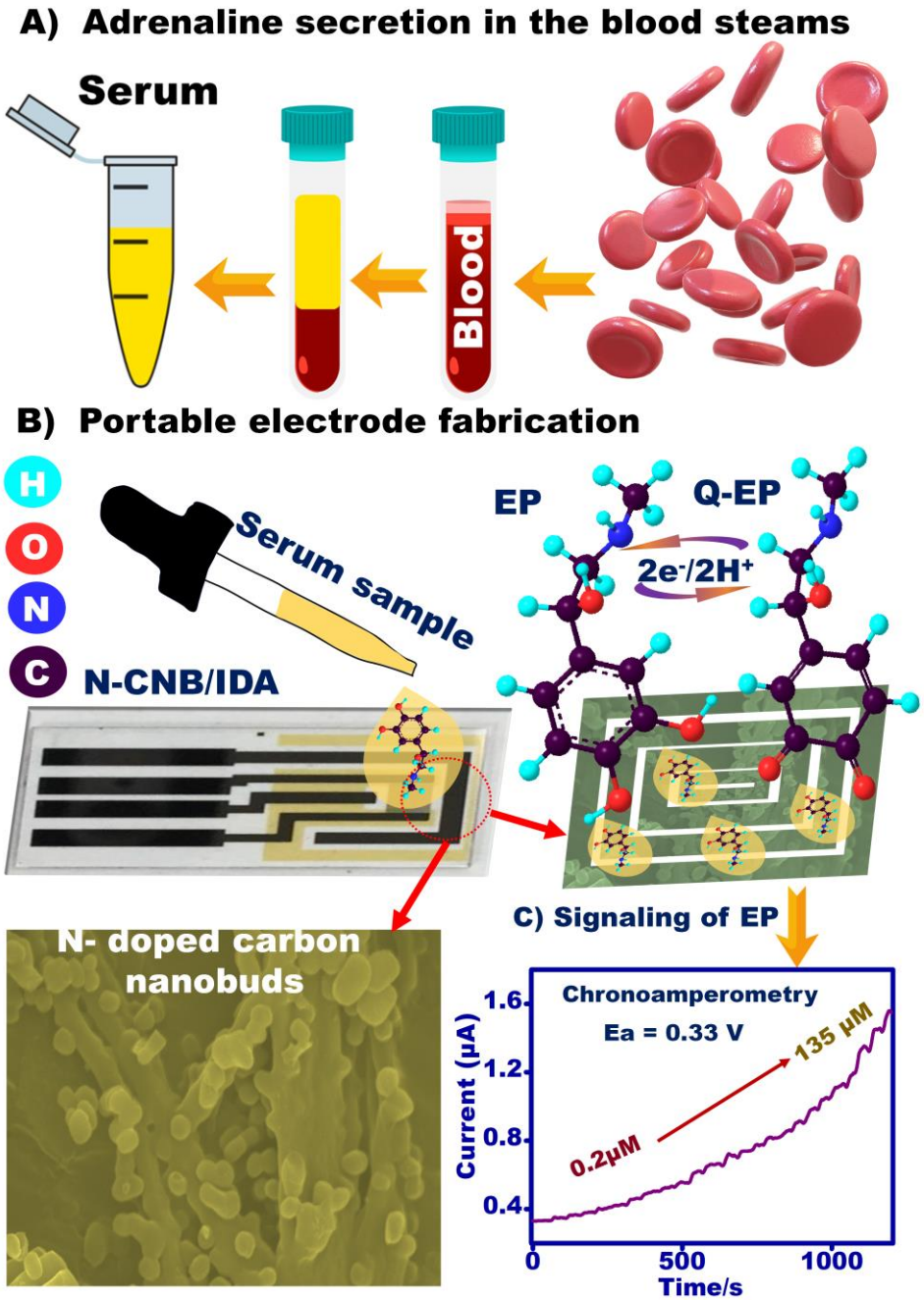

Scheme 2. The schematic design of the EP sensing in human serum samples using the N-CNB/IDA chipset nanosensor. A) the Human serum sample preparation after centrifuging of the whole blood. B) On-site detection of EP after adding 10 µL of the serum sample at the chipset electrode. C) Electrochemical signaling of EP concentrations in the samples using chronoamperometry techniques.

Table 1: Determination of EP in human serum samples. EP quantitative analyses were carried out by spiking it with a concentration in the range of 0.05 - 0.25 µmol L^{-1}. The standardization analyses of targets were determined according to amperometry techniques at 0.26 V and repeated 3 times per each sample analysis. Not %Recovery is the percentage of recovery (%R= C_A/C_F x 100).

	EP added/ µL	***EP found/ µL***	***% Recovery***
Serum sample	0.5	0. 486 ± 0.002	97.2
	1	0.984 ± 0.001	98.4
	1.5	1.462 ± 0.002	97.5
	2	1.986± 0.003	99.3
	2.5	2.482± 0.004	99.28

Mohammed Y. Emran, Sherif A. El-Safty*, Ahmed Elmarakbi, Abduallah Reda, Ayman EL Sabagh, Mohamed A. Shenashen

Chipset nanosensor based on N-doped carbon nanobuds for selective screening of epinephrine in human samples

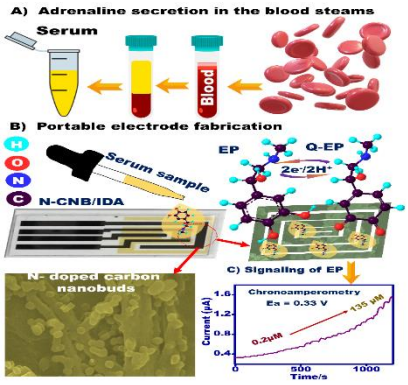

Portable epinephrine (EP) biosensor has been designed based on N-doped carbon nanobuds decorated the interdigitated electrode array (IDA). The EP biosensor of N-CNB/IDA shows highly sensitive and selective assay for screening the EP-molecules in human fluids (i.e., human serum sample)